The Journal of Experimental Biology 210, 2767-2780
Published by The Company of Biologists 2007
doi:10.1242/jeb.000265

Commentary

Fish biorobotics: kinematics and hydrodynamics of self-propulsion

George V. Lauder[1,*], Erik J. Anderson[2], James Tangorra[3] and Peter G. A. Madden[1]

[1]*Museum of Comparative Zoology, Harvard University, 26 Oxford Street, Cambridge, MA 02138, USA,* [2]*Department of Engineering, Grove City College, 100 Campus Drive, Grove City, PA 16127, USA and* [3]*Bioinstrumentation Laboratory, Massachusetts Institute of Technology, 77 Massachusetts Avenue, Cambridge, MA 02139, USA*

*Author for correspondence (e-mail: glauder@oeb.harvard.edu)

Accepted 25 April 2007

Summary

As a result of years of research on the comparative biomechanics and physiology of moving through water, biologists and engineers have made considerable progress in understanding how animals moving underwater use their muscles to power movement, in describing body and appendage motion during propulsion, and in conducting experimental and computational analyses of fluid movement and attendant forces. But it is clear that substantial future progress in understanding aquatic propulsion will require new lines of attack. Recent years have seen the advent of one such new avenue that promises to greatly broaden the scope of intellectual opportunity available to researchers: the use of biorobotic models. In this paper we discuss, using aquatic propulsion in fishes as our focal example, how using robotic models can lead to new insights in the study of aquatic propulsion. We use two examples: (1) pectoral fin function, and (2) hydrodynamic interactions between dorsal and caudal fins. Pectoral fin function is characterized by considerable deformation of individual fin rays, as well as spanwise (along the length) and chordwise (across the fin) deformation and area change. The pectoral fin can generate thrust on both the outstroke and instroke. A robotic model of the pectoral fin replicates this result, and demonstrates the effect of altering stroke kinematics on the pattern of force production. The soft dorsal fin of fishes sheds a distinct vortex wake that dramatically alters incoming flow to the tail: the dorsal fin and caudal fin act as dual flapping foils in series. This design can be replicated with a dual-foil flapping robotic device that demonstrates this phenomenon and allows examination of regions of the flapping performance space not available to fishes. We show how the robotic flapping foil device can also be used to better understand the significance of flexible propulsive surfaces for locomotor performance. Finally we emphasize the utility of self-propelled robotic devices as a means of understanding how locomotor forces are generated, and review different conceptual designs for robotic models of aquatic propulsion.

Key words: fish, swimming, robotics, locomotion, flow visualization, digital particle image velocimetry, kinematics, fin, foil, propulsion.

Introduction

The comparative biomechanics and physiology of moving through water has long attracted the attention of both biologists and engineers, and recent decades have witnessed considerable growth in the study of aquatic animal locomotion. Major results of these efforts include a much more complete understanding of how animals moving in the water use their muscles to power movement, detailed descriptions of body and appendage motion during propulsion, and experimental and computational analyses of fluid movement and the attendant forces (for reviews, see Biewener, 2003; Fish and Lauder, 2006; Lauder, 2006; Lauder and Drucker, 2004; Shadwick and Lauder, 2006). Although a number of areas remain in which currently dominant approaches can still yield fruitful new insights (including, for example, analyses of maneuvering locomotion, how animals effect control of multiple locomotor surfaces to maintain stability, and examination of locomotor repertoires used by animals in natural flow regimes), it is clear that substantial future progress in understanding aquatic propulsion will require new lines of attack.

Fortunately, recent years have seen the development of one such new avenue that holds considerable promise for testing classical hypotheses, as a source of new data on aquatic locomotion, and as a novel direction that greatly broadens the scope of intellectual opportunity available to researchers: the use of biorobotic models. Robotic models of body and appendage function, with the attendant ability to program specified motions, the intrinsic abstraction from detailed morphological features present in individual species, and the ability to explore a broader parameter space of movement than exists in nature, allows investigators to explore the biomechanics of aquatic propulsion in wholly new ways. Recent investigations into aquatic biorobotics include (Alvarado and Youcef-Toumi, 2005; Anderson and Chhabra, 2002;

Bandyopadhyay, 2005; Kato, 2000; Liu and Hu, 2006; Long et al., 2006a; Long et al., 2006b; Low, 2006; Tangorra et al., 2007b; Triantafyllou and Triantafyllou, 1995). Comparative approaches that examine locomotor function in different species, while invaluable, are limited by the investigator's inability to control for the many non-locomotor differences among these species. Furthermore, it is difficult to alter the natural motions of the body and appendages in freely swimming animals to examine the effect of novel movement patterns on locomotor performance. And, robotic models can have their structure and material properties (such as flexibility) altered at will, allowing a controlled investigation of the locomotor performance effects of such changes.

Interest in fish biorobotics is not new, and there is a long history, dating back to early experimental work using models (Houssay, 1912; Breder, 1926; Gray, 1953). These investigators constructed mechanical models that allowed them to investigate power output, undulatory wave formation, and the function of the tail during fish locomotion (for a review, see Alexander, 1983), which greatly increased our early understanding of how fishes generate propulsive forces.

Robotic models can be used to special advantage when coupled closely with experimental studies of freely swimming animals. This allows direct comparisons to be made between the function of models with various configurations and the function of biological designs, and ensures reasonable comparison of the performance spaces of the robotic models and natural locomotion. In our view, the marriage of robotic models with experimental analyses of biological locomotion promises to drive the next set of major advances in our understanding of aquatic propulsion.

In this paper we discuss, using aquatic propulsion in fishes as our focal example, how such a research program might lead to new insights in the study of aquatic propulsion. Key questions that can be studied using robotic models of fish propulsion include the following. How do fins generate thrust? How do multiple fins arrayed along the body of fishes interact hydrodynamically? How does flexiblity of the propulsive surface affect the speed and efficiency of locomotion? And, do fishes use kinematic patterns that generate maximal thrust, or would different motions, if biologically possible, improve locomotor performance?

We use two specific examples: (1) pectoral fin function and (2) hydrodynamic interactions between dorsal and caudal fins. We first present kinematic and hydrodynamic data from experimental studies of fish pectoral, dorsal and caudal fins to provide the biological context, and then present data from a robotic model of the pectoral fin and from a flapping foil robotic device that models dorsal–caudal fin interactions and allows investigation of the propulsive properties of flexible foils. We emphasize the utility of *self-propelled* robotic devices as a means of understanding how locomotor forces are generated, and review different conceptual designs for robotic models of aquatic propulsion.

Fish locomotion: function of paired and median fins *in vivo*

Fish generate propulsive forces and control body position through motions of their body and median and paired fins (Lauder, 2006; Webb, 2006). Each of the fins that act as control surfaces during locomotion possess distinct skeletal supports and associated intrinsic musculature that provide active control of fin surface movement (Fig. 1). In addition, ray-finned fishes (but not sharks) have the ability to actively control the surface conformation of their fins *via* a unique bilaminar fin ray design, which allows musculature at the base of the fin to generate curvature of the fin rays along their length, and thus resist hydrodynamic loading (Alben et al., 2007; Lauder and Madden, 2006; Lauder et al., 2006). The pectoral fins of fishes are paired structures, while the dorsal, anal and caudal fins are midline structures (Fig. 1). Although fluid dynamic interactions between the paired pectoral fins and more posterior median fins are theoretically possible, no such interactions have been demonstrated experimentally, and we will treat the two sets of fins separately here. The dorsal and anal median fins generate flows that interact with the caudal fin (Drucker and Lauder, 2001; Drucker and Lauder, 2005; Standen and Lauder, 2007), and thus the median fins need to be considered as a group.

We first consider the kinematics and hydrodynamics of pectoral fin propulsion, before considering the function of the dorsal and caudal fins.

Paired fin propulsion: pectoral fins

The pectoral fins of fishes can undergo considerable deformation during the fin beat cycle, and the recent availability of megapixel resolution high-speed video has allowed detailed quantification of fin surface bending and the motion of individual fin rays (Lauder et al., 2006; Standen and Lauder, 2005). For example, in bluegill sunfish (*Lepomis macrochirus*) swimming at a slow speed (0.5 L s^{-1}, where L is total length) involving only use of the pectoral fins, the area of the fin changes by approximately 30% as the fin rays separate, and there is considerable fin twisting as well as chordwise and spanwise bending (Fig. 2). During abduction as the pectoral fin moves away from the body, the fin root assumes a cupped shape (Fig. 2B, posterior view), resulting in two simultaneous leading edges, while the area expansion and fin curvature is clearly seen on the return stroke (Fig. 2C).

The cupping of the pectoral fin during the outstroke is also clearly visible in laser images, which permit particle image velocimetry analyses of water flow induced by fin motion (Fig. 3) (Drucker and Lauder, 1999; Drucker and Lauder, 2002; Lauder and Drucker, 2002; Lauder and Tytell, 2006). Analyses of pectoral fin water flow patterns show that on both the fin outstroke and return stroke, water is accelerated downstream at a velocity greater than free-stream, indicating that thrust is produced by the pectoral fin throughout the fin beat cycle (Fig. 3E,F). This conclusion is corroborated by computational analyses of pectoral fin function (Mittal et al., 2006), which demonstrated two distinct thrust peaks, one each on the outstroke and the return stroke of the fin.

Median fin propulsion: the body, dorsal and anal fins

The prominent median fins (dorsal, anal and caudal) of fishes (Fig. 1) play an important and active role in locomotor dynamics (Arreola and Westneat, 1997; Drucker and Lauder, 2001; Hove et al., 2001; Jayne et al., 1996; Lauder et al., 2002; Standen and Lauder, 2005; Tytell, 2006). In many

spiny-finned fishes the dorsal and anal fins are composed of an anterior spiny portion and a more flexible posterior region, often termed the soft dorsal and anal fins (Fig. 1). The spiny portions of these fins can be erected and depressed but not moved laterally, while the soft dorsal and anal fins possess inclinator musculature that powers lateral movement (Geerlink and Videler, 1974; Jayne et al., 1996). The inclinator muscles are active during both steady swimming and maneuvering, and movement of the dorsal and anal fins generates a vortex wake (Fig. 4). Together, the dorsal and anal fins in bluegill sunfish contribute as much locomotor force during slow swimming as the tail (Tytell, 2006). Perhaps the most important consequence of the dorsal and anal fin vortex wake is that the caudal fin moves through water that has a greatly altered flow structure compared to undisturbed free-stream flow, far away from the swimming fish. Experimental studies of trout and bluegill sunfish (Drucker and Lauder, 2001; Drucker and Lauder, 2005; Standen and Lauder, 2007) show that the dorsal and anal fins produce vortices that pass downstream and are encountered by the caudal fin as it sweeps from side to side (Fig. 4). These vortices can potentially enhance thrust produced by the tail if they encounter the tail at an appropriate phase of movement. Akhtar et al. (Akhtar et al., 2007) showed through a computational fluid dynamic analysis of the sunfish dorsal fin and tail that the phase relationships reported by Drucker and Lauder (Drucker and Lauder, 2001) did indeed produce enhanced thrust by enhancing the leading edge vortex as the tail surface is inclined forward.

Another significant finding of experimental studies of median fin function is the strong side force component of the wake. This result can be seen in Fig. 4, where the dorsal fin wake generates flows that are nearly orthogonal to the free-stream. The caudal fin is also capable of generating a thrust wake signature, with a momentum jet formed at nearly a 45° angle to the direction of travel (Fig. 4C). However, a thrust wake is not present in steadily swimming anguilliform fishes, and the difference among fish wake flow patterns may be related to the three-dimensional body shape and the presence of a discrete propeller-like caudal fin (Lauder and Tytell, 2006).

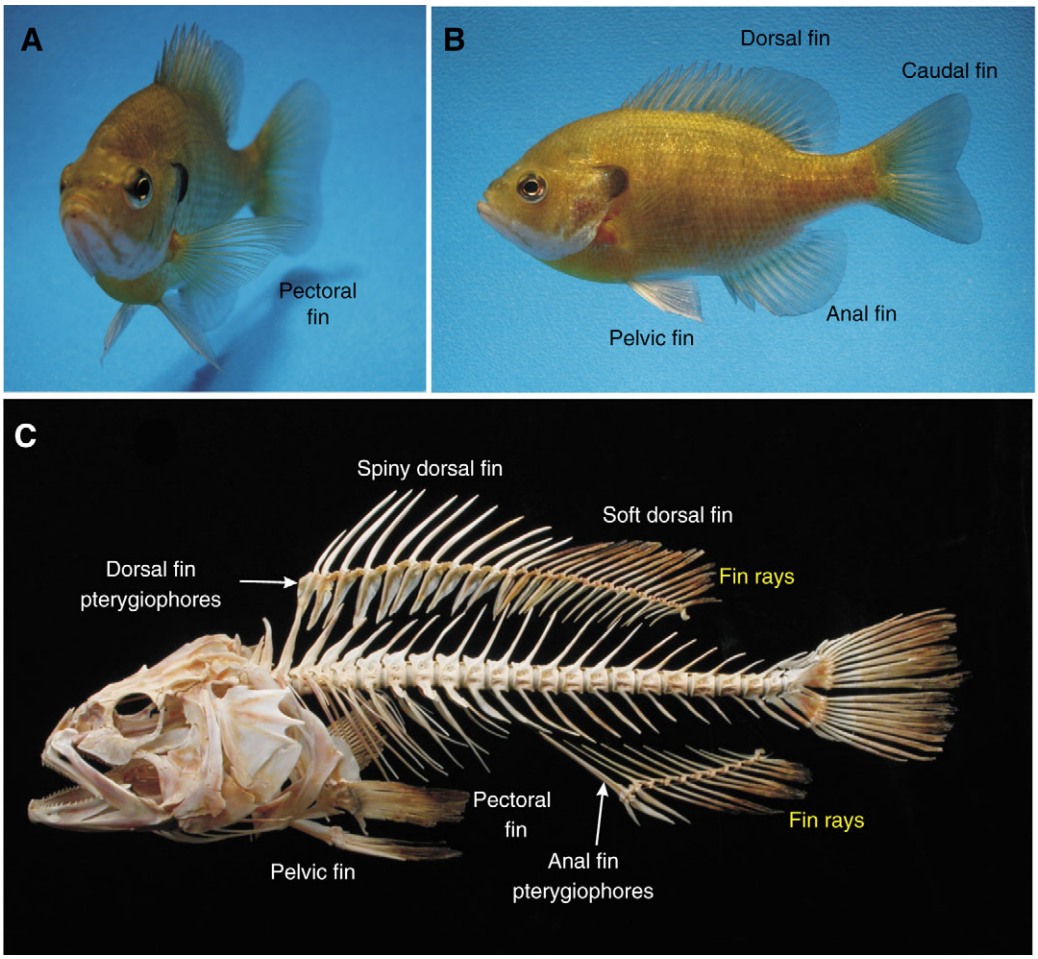

Fig. 1. (A,B) Bluegill sunfish *Lepomis macrochirus*, hovering in still water, and (C) snowy grouper *Epinephelus niveatus* skeleton, showing the positions of the major fins and their internal skeletal supports. The pectoral and pelvic fins are paired, while the dorsal, anal and caudal fins are median (midline) fins. The dorsal and anal fins of ray-finned fishes have internal skeletal supports (pterygiophores), which support musculature that moves the fin rays. Fin rays are labeled in yellow for the dorsal and anal fins. The caudal fin also has a complex series of intrinsic musculature that allows fishes to actively control tail conformation (Drucker and Lauder, 2001; Lauder, 1982; Lauder, 1989). Metal supporting elements for the grouper skeleton have been digitally removed for clarity.

Fish locomotion: studied with robotic models

The study of fish locomotor physiology and biomechanics is greatly enhanced by the ability to manipulate movement patterns experimentally in ways not possible to achieve through comparative analyses of living fishes, and to directly measure forces produced by fin-like flapping foils.

A variety of different fish robotic designs have been produced, and among the most well known are the autonomous robotic fish-like devices (Anderson and Chhabra, 2002; Kato, 2000; Liu et al., 2005; Long et al., 2006b). But much of the progress in fish biorobotics has occurred through the use of laboratory models in still water or flow tanks that allow controlled study of specific movement patterns and simultaneous force measurement.

Fig. 5 summarizes several alternative concepts for robotic platforms useful for the study of fish locomotor mechanics. One common approach is to attach a robotic fish-like device to a carriage and tow this carriage through a water tank (Fig. 5A). Under these conditions, force and torque sensors can be used to quantify the lift and thrust forces produced by the model when it is towed through the water at known speeds (e.g. Barrett et al., 1999; Triantafyllou and Triantafyllou, 1995). This approach

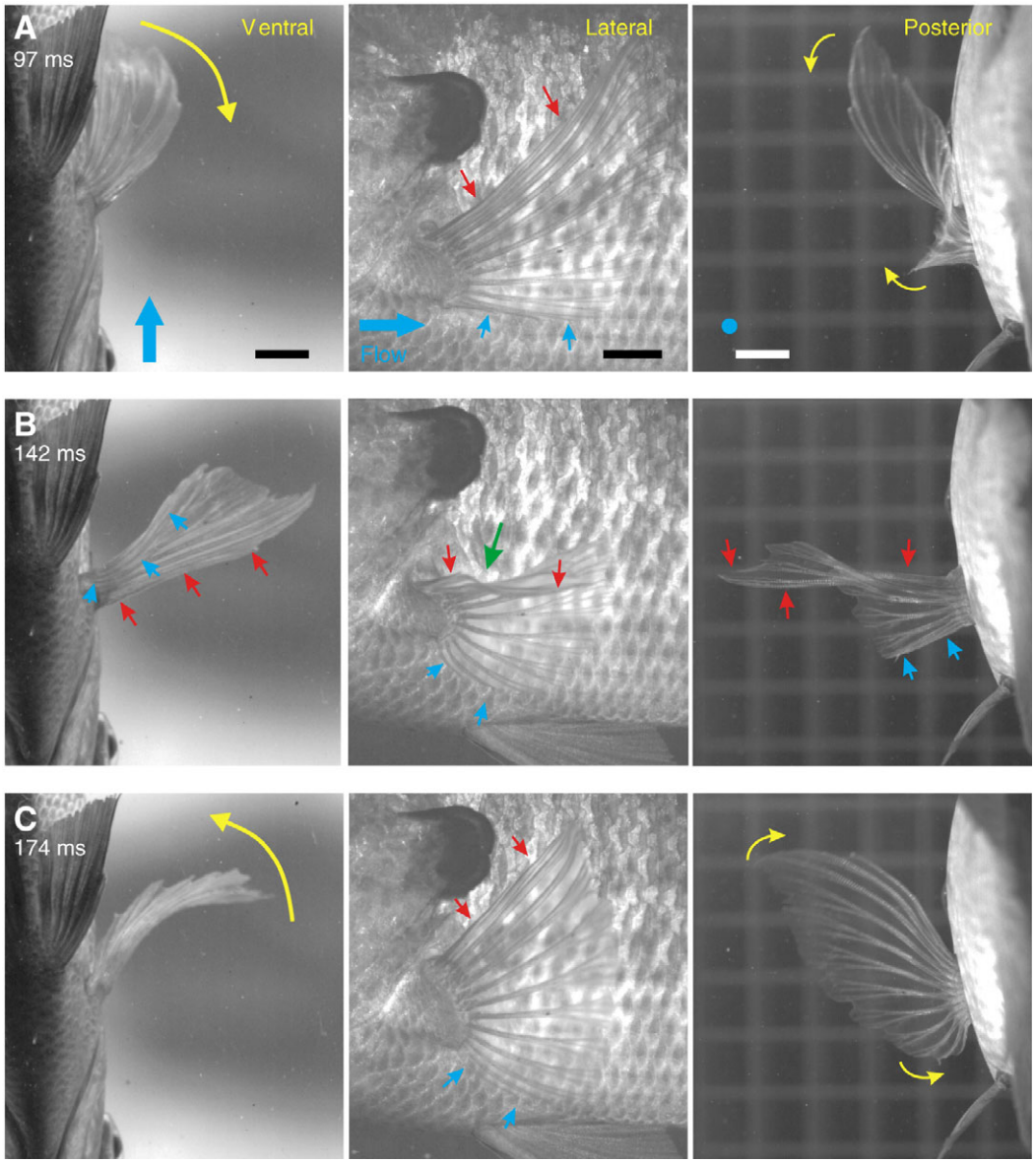

Fig. 2. Motion of the pectoral fin in a bluegill sunfish (17 cm total length, L) during steady locomotion at 0.5 L s^{-1}. Each row shows frames from simultaneous lateral, ventral and posterior digital videos (taken at 250 Hz) at three time intervals, 97 ms (A), 142 ms (B) and 174 ms (C), during a single pectoral fin beat. Yellow arrows indicate the major fin motions (smaller amplitude movements of the fin surface are not labeled with yellow arrows), the small red and blue arrows show the position of the upper (dorsal) and lower (ventral) pectoral fin edges respectively, and the green arrow shows the location of the 'dimple' on the dorsal fin margin that forms as a wave of bending passes out along the fin from base to tip. The large blue arrows and dot in A show the direction of water flow, which is perpendicular to the page in the posterior view. Note the considerable twisting and bending of the fin, and the cupped shape as the upper and lower fin margins move away from the body at the same time (A: posterior view). The fin beat begins at time 0 ms. Scale bars, 1.0 cm.

has been used in many studies of flapping foil-based propulsion and to evaluate the effect of locomotion in the wake of upstream bluff bodies such as a cylinder or rock placed in the flow (e.g. Beal et al., 2006; Hover et al., 2004; Techet et al., 1998).

Another approach, illustrated in Fig. 5B, is to allow the robotic models to self-propel. Under the condition of self-propulsion at a steady speed, the thrust generated by the model must equal the drag force experienced by the robotic device. In the robotic devices described in this paper, self-propulsion is allowed by mounting the carriage holding the device motors on extremely low friction air bearings. These air bearings permit motion in the upstream–downstream direction but not side-to-

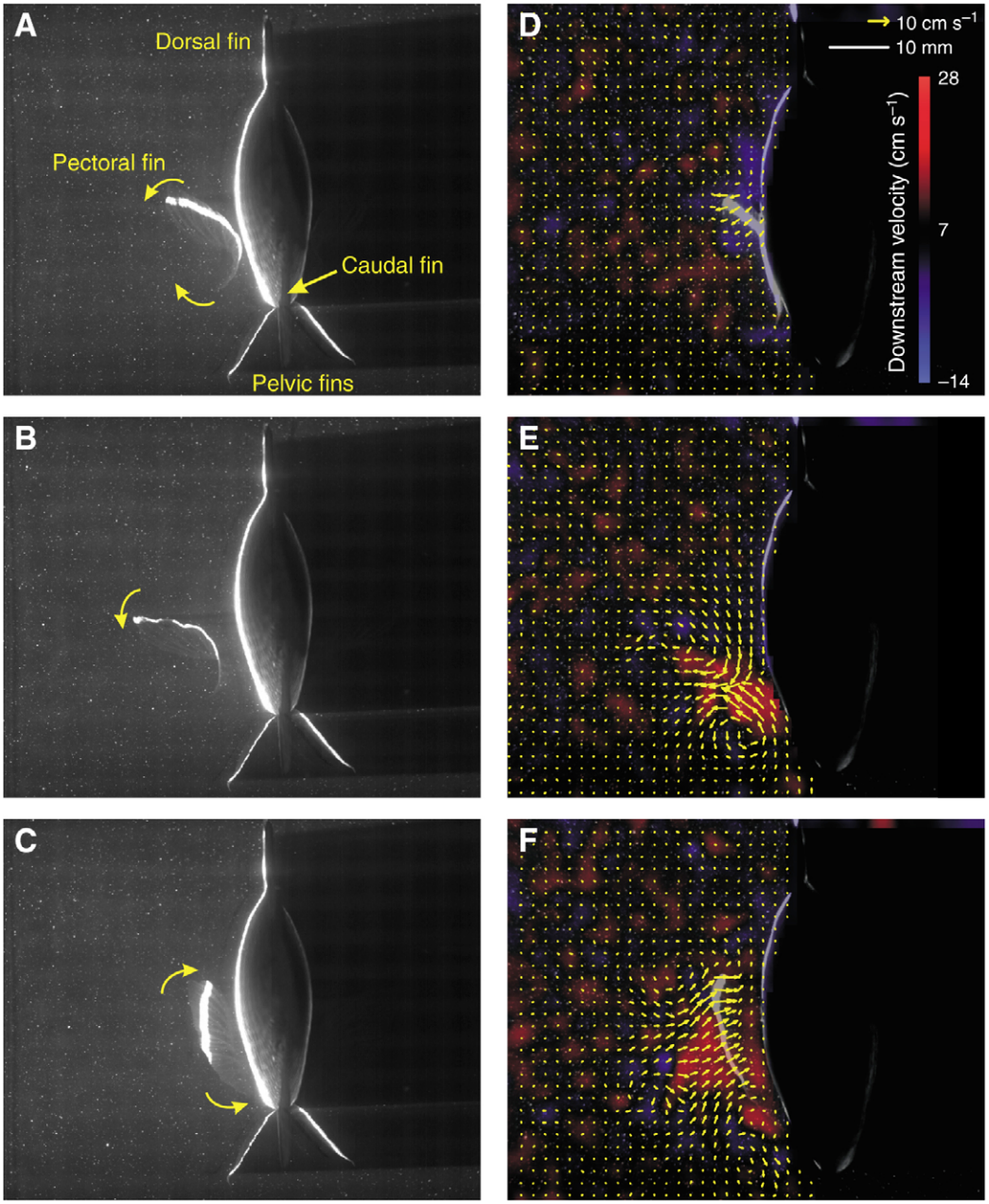

Fig. 3. Hydrodynamic function of the pectoral fin in bluegill sunfish swimming at 0.5 L s^{-1}, as seen in posterior view looking upstream. A laser-generated sheet of light illuminates a thin slice of water flow as well as the pectoral fin and body, which casts a shadow to the right. Laser light penetrates the translucent fin, allowing flow between the fin and the body to be quantified. Water flow in this figure is out of the page, toward the reader. Images were obtained from 500 Hz digital video. (A–C) Particle image velocimetry images showing the movement of the fin illuminated by the laser light sheet in relation to the body and position of the other fins. Duration of movement shown=0.48 s from panels A–C. Yellow arrows show the key fin movements: note the cupped fin shape in A and B. (D–F) Water flow patterns as a result of pectoral fin movement. This column is from a different sequence than the frames in the left column. Yellow arrows indicate water velocities (every other vector is shown), and the background color scheme is coded so that black color indicates free stream flow velocity (7 cm s^{-1}), red color flow accelerated by the fin to greater than free stream velocity, and blue color showing flow slowed below free stream. Note that the pectoral fin accelerates flow on both the outstroke and return stroke (red color in E and F).

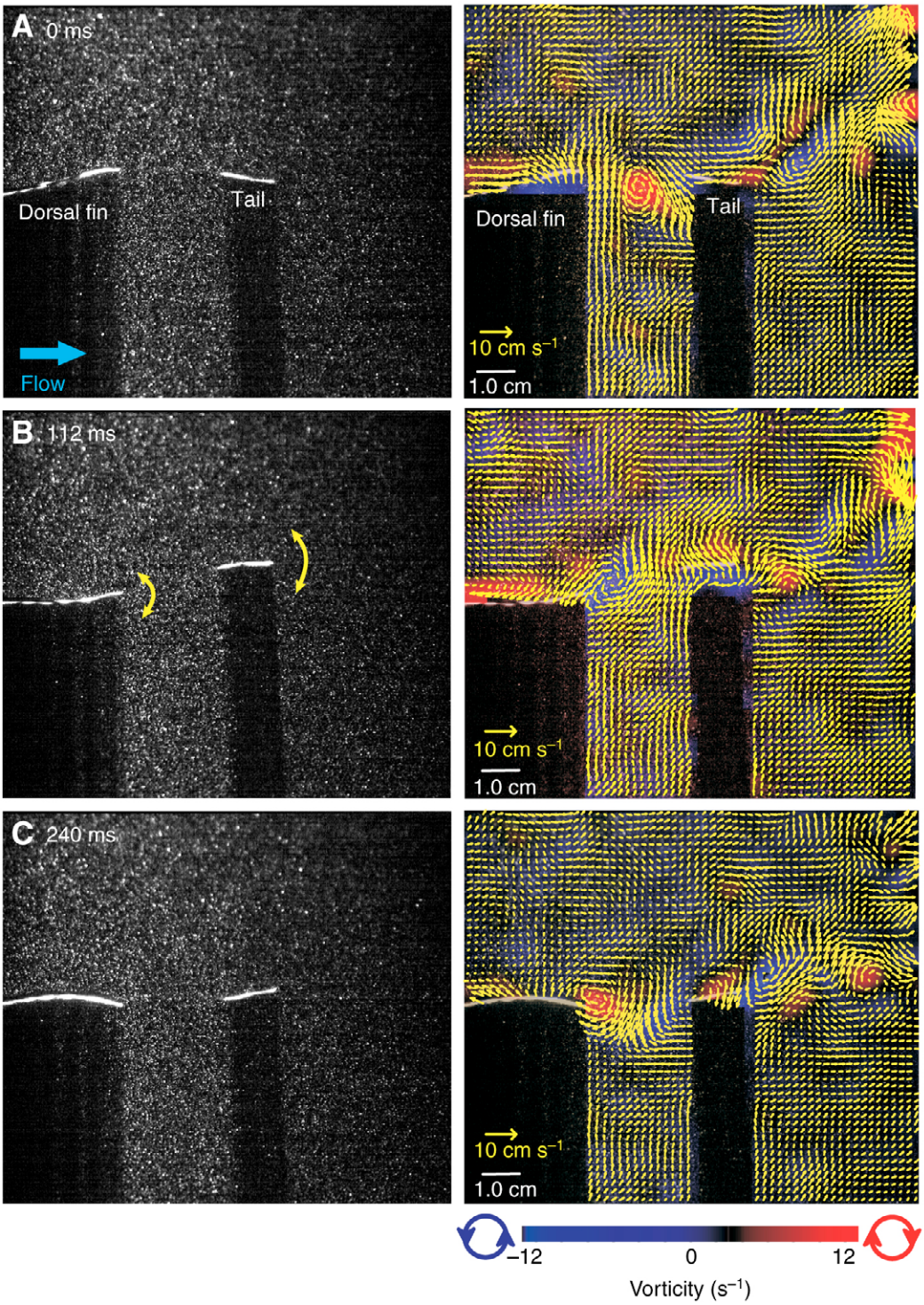

Fig. 4. Hydrodynamic analysis of the dorsal fin and caudal fin in swimming bluegill sunfish, to show that these two fins can act as dual flapping foils in series, and that flow leaving the dorsal fin can affect caudal fin function. The caudal fin of ray-finned fishes does not move through undisturbed free stream flow, but rather has its flow environment highly modified by upstream fins. The left panels show the laser-imaged dorsal fin and tail of a bluegill sunfish (16.5 cm *L*) swimming at 17 cm s^{-1}; laser light illuminates from top to bottom in these images, and the dorsal fin and tail cast shadows toward the bottom. Yellow arrows in B show the left–right oscillatory motion of the dorsal fin and tail as seen from above. In the right panels these images are analyzed to show water flow velocities around the fins (vectors were not calculated in the fin shadows) and vorticity. The views shown in this figure are from above, looking down on the upper surface of the fish with the dorsal fin and tail (also see Fig. 1). In A, the dorsal fin has shed a clockwise vortex that is moving toward the tail. This vortex passes above the tail (B) while the dorsal fin sheds a new vortex of opposite sign on the return stroke. This pattern repeats as a clockwise vortex is just leaving the dorsal fin again (C). Note that flow in the gap between the dorsal fin and tail is nearly orthogonal to free-stream flow. Free-stream flow has been subtracted from the right panel images to reveal flow structure; images on the left have been contrast-enhanced.

side movement of the whole carriage (although heave motors do move the fin-like foils from side to side). The flapping surface is immersed into a flow tank, and the speed of the external flow adjusted so that the flapping robotic device generates sufficient thrust to precisely hold position at a mean fixed position. When the robotic device holds at an equilibrium position in the flow tank (termed X_{eq}), the flow speed is noted as U_{eq} (Fig. 5Bi). Different phase relationships between heave and pitch movement will give rise to different U_{eq} values for which the robotic device holds position at X_{eq}.

Once U_{eq} has been determined for a given set of movement parameters, the robotic device can be attached to a force transducer at position X_{eq} to allow quantification of thrust, lift, and side forces at this equilibrium position under imposed flow of U_{eq} (Fig. 5Bii). By measuring forces at known self-propelled speeds, forces are measured under conditions at which mean thrust must equal mean stroke-averaged drag. One issue of practical concern is the force generated by the cable bundle that is necessary to provide power to the motors and to read data from the force, torque and position sensors. The effect of the cable bundle can be minimized by using an X_{eq} value that corresponds to the neutral position of the carriage on the air bearings: if all measurements are made at this neutral X_{eq} measured under conditions of no flow, then the cables have no effect on the final measured U_{eq} and force values.

A robotic fish pectoral fin

We have constructed a self-propelled robotic pectoral fin that replicates many of the anatomical features of a real fish pectoral fin (Fig. 6). This biorobotic pectoral fin is attached to a carriage that is itself mounted on air bearings that have very low friction for motion in the upstream–downstream direction (Fig. 6A). The pectoral fin robot uses motor-driven nylon tendons to actuate bilaminar fin rays (each ray is composed of two halves, or hemitrichs) (Lauder, 2006) that are of similar design to real fish fin rays: displacement of one half of the ray induces a curvature in the ray, and curvature of the whole fin surface can be controlled by producing curvature in all rays. Like the biological fin ray, small displacements at the base cause a large displacement at the tip of the fin ray. The whole fin can be reoriented by moving a compliant base (Fig. 6B). In the design of the biorobotic fin we used five bilaminar fin rays embedded in a flexible urethane webbing with a modulus of elasticity of approximately 0.10 MPa, similar to that of the (relatively extensible) fin membrane in bluegill sunfish (Lauder et al., 2006). The webbing is pleated so that it can be expanded easily. The complex geometry of the fin rays and fin ray base plate (Fig. 6C) was manipulated to adjust the fin ray's passive stiffness and ability to curl when the bases of the hemitrichs were displaced, and they were constructed using stereolithography (which allowed rapid polymerization of different prototype ray structures). Nylon tendons are attached through small holes in the base of the hemitrichs.

The compliant base mechanism supports the fin rays and serves as a deformable joint about which the fin rays are moved. Fin rays are held in place by tension in the nylon tendons. A stiff base plate (Fig. 6B,C) is mounted between the compliant base mechanism and the actuators and contains channels through which the tendons pass. The compliant base has multiple segments designed to allow it to bend and generate a range of biologically realistic motions that would be difficult to

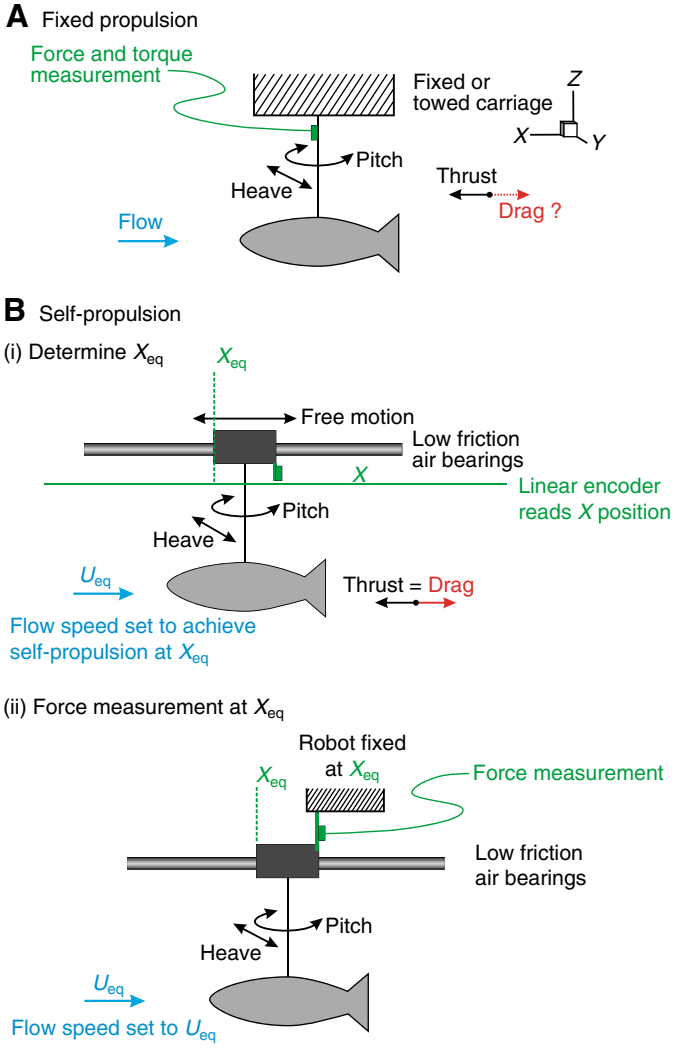

Fig. 5. Schematic figure to illustrate two different categories of fish-like aquatic robot design and the measurements that might be made from each design. (A) Robot is attached to a sting (a rod holding the robotic model vertically from the carriage above) and either fixed in place while forces are measured on the sting, or towed at a fixed velocity on a moving carriage. In either case, the robot is not self-propelled, but rather moves at externally imposed speed. In this case, there need be no equality between thrust and drag forces, as it is not known if the robot is generating sufficient thrust to overcome drag. (B) Robot swims at a self-propelled time-averaged constant speed as a result of thrust generated by heave and pitch motions, and mean thrust force per cycle must equal the mean drag force. The flow speed in the tank is adjusted to a value, U_{eq}, where the robot propels itself at a constant equilibrium X position, termed X_{eq}. The robot is free to move itself upstream and downstream on a low friction air bearing system. Once X_{eq} is determined for a particular heave and pitch motion pattern during self-propulsion, the robot can be fixed in position at X_{eq} to measure forces and torques while the same motion pattern and flow speed used for self-propulsion are imposed. This allows force measurement under conditions identical to self-propulsion, when thrust and drag forces must be equal.

achieve with a rigid hinged mechanism (Fig. 6D–G): expansion and hence area increase, curling of the surface, and cupping (similar in character to motions of the sunfish pectoral fin during locomotion, Figs 2, 3).

When the carriage supporting the fin is mounted above the flow tank (Fig. 6A), the biorobotic fin in the tank can be imagined to represent the pectoral fin of a fish swimming on its side just below the water's surface. The design allows the submerged fin to be reoriented through ±60° pitch and 180° yaw. To measure thrust force, the fin carriage was mounted on the air bearings in an equilibrium position and attached to a force transducer (as in Fig. 5Bii). The force produced by the biorobotic fin along the *X* axis (fore and aft) was measured during fin beats as the fin was cycled between approximately 0° (horizontal or 'against the fish body') and 90° (vertical or 'maximum outstroke'). The fin's movements were created by superimposing combinations of curl, expansion and cupping onto a basic sweep motion. Simple sinusoids were used to drive the sweep, curl and expansion motions at about 0.60 Hz. Cupping was activated using a square wave with the fin cupped during out-stroke and flat during in-stroke. Since the commanded velocity was the same on the out-stroke and in-stroke, changes in force were related directly to changes in the fin's shape and its effect on the water. All tests on the robotic fin shown in Fig. 6 were conducted in still water.

Robotic pectoral fin forces produced under three different movement patterns are shown in Fig. 7. The most biologically realistic movement pattern is the 'cup and sweep', which is the closest to the pattern observed in sunfish (Fig. 2). The pectoral fin is cupped as it sweeps out from the body and flattens as it sweeps back on the return stroke (Fig. 2A). The

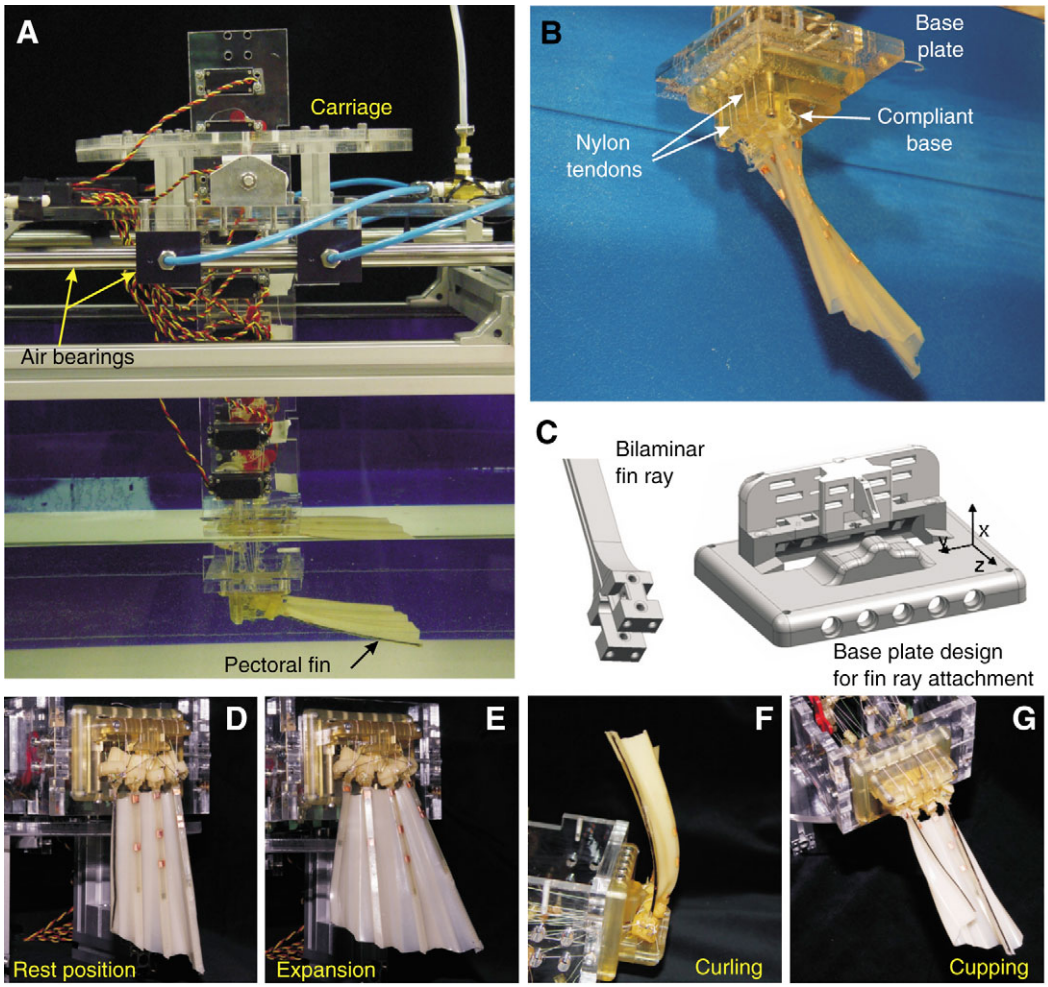

Fig. 6. Design of the self-propelled robotic pectoral fin with bilaminar fin rays. (A) Carriage that holds the robotic fin mounted above the flow tank on air bearings that allow horizontal translation in the *X*-direction with little friction. The pectoral fin can be seen submerged in the flow tank below the array of black actuating motors. (B) Base plate that holds the fin and compliant base support, and guides the nylon tendons to the fin rays. (C) Design of the base plate and the bilaminar fin rays that mimic the curvature control of fin rays in fin ray-finned fishes (Alben et al., 2007; Lauder, 2006). Note the two separate heads for each half of the fin ray, which receive separate nylon tendons. (D–G) Motion of the robotic pectoral fin from the rest position to show expansion, curling and cupping of the fin. Black lines have been drawn on the two leading edges of the fin to more clearly show the motion in F and G. Cupping, bending and expansion of the bluegill sunfish fin, as shown in Figs 2 and 3, are well replicated by the robotic model. Pectoral fin rest length=12.8 cm at the longest ray; fin width at base and tip is 5.5 cm and 8.0 cm, respectively. The base plate is 5.5 cm×8.5 cm. The fin rays vary from 9.0 cm to 12.5 cm long and the rays are 0.1 cm thick and 0.4 cm wide.

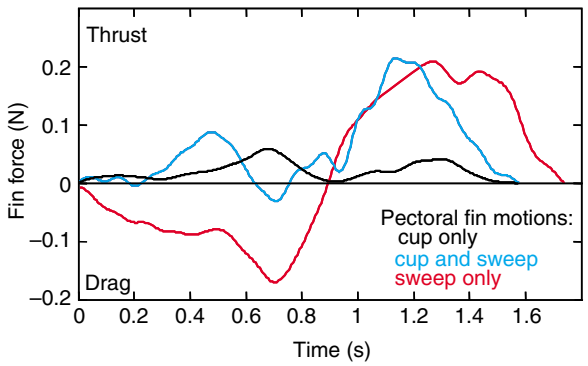

Fig. 7. Force in the *X*-direction (see Fig. 5) reflecting thrust and drag, measured from the robotic pectoral fin during a single fin beat under three different imposed movement patterns (shown in different colors). Robotic models of the pectoral fin allow analysis of the effects of different movement patterns in a way not possible with studies of live animals alone. When the fin executes a cupping motion only (black trace), a force curve with two distinct peaks is produced with no drag force at the transition from outstroke (abduction) to instroke (adduction). A cupping and sweeping motion (blue trace) generates considerably higher thrust forces as well as a small drag force during the transition. Moving the fin in sweep only (red trace), produces large drag forces on the outstroke and roughly equivalent thrust on the return stroke.

cup and sweep motion generates a biphasic thrust trace, with one thrust peak during abduction (out-stroke) and a second peak during adduction (in-stroke). This closely resembles the force pattern calculated using computational fluid dynamics based on the actual movement of sunfish pectoral fins (Lauder et al., 2006; Mittal et al., 2006), and the experimental observation that thrust is produced throughout the fin beat (Fig. 3) (Lauder and Madden, 2006; Lauder et al., 2006). There is a small period of drag for the cup and sweep motion near mid-stroke that corresponds to the time when the pectoral fin is changing from abduction to adduction (Fig. 7). Interestingly, two (smaller) peaks in thrust force are obtained with a cupping only movement and the small period of net drag force is absent. This suggests that the observed cupping motion of the bluegill pectoral fin is an important component of thrust generation. Thrust production during initial cupping may reflect the dual leading edge vortices observed during cupping in bluegill sunfish fins (Lauder et al., 2006). In contrast, for a sweep motion without cupping, large drag forces are generated on the outstroke, while thrust is generated on the return. Little net thrust is produced by the sweep-only motion (Fig. 7).

There are several noteworthy differences between the function of the robotic pectoral fin and that of sunfish. Most importantly, we observed no wave of spanwise bending along the robotic fin (e.g. Fig. 2B), and this may be due in part to the relatively stiffer fins rays in the robotic model. Bluegill sunfish fin rays and membrane have an elastic modulus of about 1 GPa and 0.3–1 MPa, respectively (Lauder and Madden, 2006), which makes sunfish fins more flexible than the robotic pectoral fin we constructed. In sunfish, relatively high fin flexibility allows generation of a chordwise wave, which may contribute to thrust production during the transition from abduction to adduction, and the lack of such motion in the robotic model may result in the small period of negative thrust at midstroke.

A flapping foil robot

The dorsal and anal fins and the caudal fin of fishes can be considered as representing dual flapping foils arranged in series (Figs 1, 4). The dorsal and anal fins constitute the upstream foil, leaving a wake encountered by the downstream caudal fin foil (Fig. 4). The pattern of median fin function in fishes observed experimentally to date involves a relatively narrow range of fin movement amplitudes and phasings (Drucker and Lauder, 2001; Drucker and Lauder, 2005; Hove et al., 2001; Standen and Lauder, 2005; Standen and Lauder, 2007), and in order to control for interspecific differences and to explore a large parameter space of heave and pitch motions, it is useful to have a robotic device that can execute programmed motions. Because the median fins of fishes are attached to the undulating fish body, only relatively small differences in phase and amplitude are observed between the dorsal, anal and caudal fins. A robotic device allows the uncoupling of the motion of the dorsal and anal fins from that of the caudal fin, and new (biologically impossible) movement patterns can be executed to examine their effect on foil thrust and on the wake patterns produced by different foil motions. A robotic flapping foil device is also useful for testing the effect of foil flexibility on wake flow patterns, for quantifying hydrodynamic foil–foil interactions, and for understanding why some movement patterns produce an anguilliform wake, while others generate the classic carangiform fish wake flow pattern (Lauder and Tytell, 2006).

We have constructed a dual-foil flapping robotic device in which two foils (we used the NACA 0012 airfoil cross-sectional geometry, which approximates the shape of many aquatic propulsive surfaces) (Fish and Lauder, 2006) are separately mounted on carriages attached to an air bearing system to allow independent self-propulsion of each foil (Fig. 8A) with little frictional loss. Linear encoders attached to each foil carriage allow measurement of foil position. During self propulsion, we measure the flow tank speed (U_{eq}) required for the foil to hold position at the equilibrium location (X_{eq}; Fig. 5B) and determine the locomotor performance of different heave and pitch amplitudes and frequencies while simultaneously quantifying the wake flow pattern generated by each foil using particle image velocimetry. Once U_{eq} is determined, we attach the foils to a force transducer at position X_{eq} and measure the force generated by each set of movement parameters. These experiments are repeated for a range of interfoil spacings, ranging from 0.5 to 2.0 chord lengths, where the chord is the width of the foil.

This flapping robotic device also allows us to investigate the locomotor properties of biomimetic foils with varying degrees of flexiblity. The role of flexibility in biopropulsion is still not well understood. Both rigid foils and flexible foils can generate thrust, but fin and body propulsion in most aquatic systems involves flexible hydrofoils. What do biological systems gain, if anything, by utilizing flexible propulsive surfaces? By mounting foils with varying degrees of flexibility on the robotic

flapping device, we can correlate self-propelled speed with flexibility while controlling all other parameters.

Here we focus first on the presentation of foil wake flow patterns during movement with 0.5 chord length spacing between the two foils under conditions of self-propulsion (Fig. 9), for comparison with the experimental data from bluegill sunfish dorsal and caudal fins (Fig. 4) and computational fluid dynamic results (Akhtar et al., 2007). The influence of the upstream foil on the flow encountered by the downstream foil is clearly evident as a stream of trailing vorticity encounters the downstream foil (Fig. 9B) as it crosses the wake of the upstream foil. Furthermore, the reduced flow between the two foils is evident, as is the enhancement of the leading edge vortex on the downstream foil (Fig. 9C). This is precisely the mechanism identified by Akhtar et al. in their computational study for thrust enhancement when the wake of the upstream foil encounters the trailing foil and causes increased leading edge suction (Akhtar et al., 2007).

The strong thrust wake of the downstream foil is also evident as the foil reaches the extremes of side-to-side motion (Fig. 9A,C) with two counter-rotating regions of vorticity and a large region of water with relatively high momentum moving back and to the side in a manner similar to the carangiform wake of swimming fishes (e.g. Nauen and Lauder, 2002a; Nauen and Lauder, 2002b).

The robotic flapping apparatus also demonstrates that a passively flexible foil can generate thrust and a wake pattern similar to that seen in swimming fishes. Fig. 10 shows self-propulsion at 24 cm s^{-1} by a flexible plastic foil actuated only in heave, a motion orthogonal to free stream flow. Thrust is generated by momentum transfer to the surrounding water as a wave of bending passes down the deforming plastic foil, and also by attached leading vortices on the forwardly inclined foil surface that remain attached for most of the movement cycle (Fig. 10A,C). The wake generated by the flexible plastic foil resembles that of anguilliform swimming in eels (Tytell and Lauder, 2004), with large laterally directed momentum jets and elongate shear layers that break up into multiple centers of vorticity (Fig. 10C).

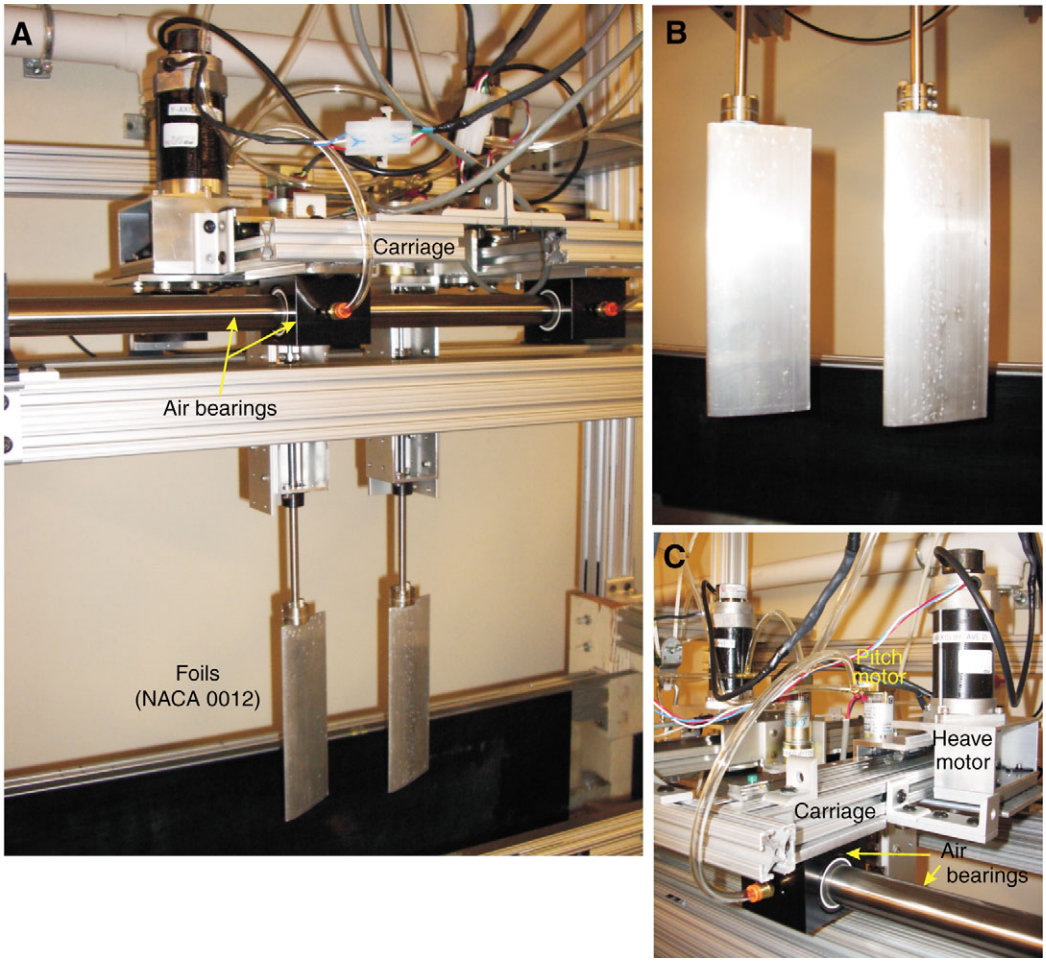

Fig. 8. Design of the self-propelled dual flapping foil robot to study fish fin function. (A) Carriage that holds the dual foils, with the heave and pitch motors for each foil mounted above the flow tank on air bearings that allow horizontal translation in the *X*-direction with little friction. This design feature is critical to allowing self-propulsion. In this image, the two foils are suspended above the flow tank. (B) Close view of the two foils (NACA 0012 in cross-sectional shape); the foils are 6.85 cm in chord length (width) and 19 cm high. (C) Close view of the pitch and heave motors for one foil mounted on the carriage and air bearing system.

Even using simple flexible foils and actuation only in heave, complex wake flows can be generated that strongly resemble fish locomotor wake patterns. Furthermore, the comparison of rigid and flexible foils (Figs 9 and 10) suggests that even simple models of flexible deforming surfaces can generate complex wake patterns with biological relevance.

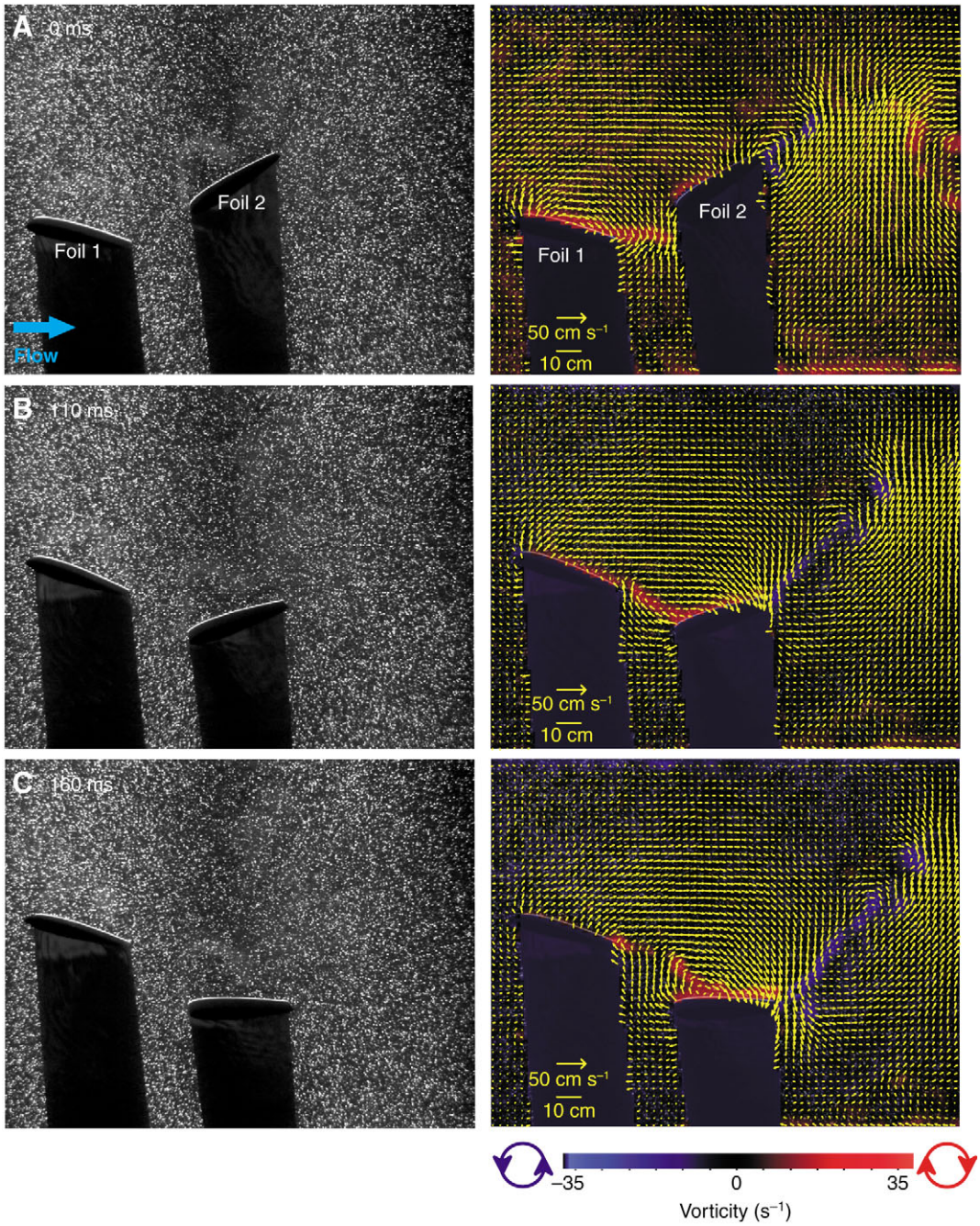

Fig. 9. Hydrodynamics of the dual flapping foil robot, self-propelling at a speed of 53 cm s^{-1}. The distance between the foils is fixed at 0.5 chord lengths. The two foils have been programmed to move in sinusoidal motion with a 140° phase lag difference between them and a period of 588 ms. The front foil has a 20° pitch amplitude and a 2.5 cm heave distance, while the rear foil moves with 30° pitch amplitude and a 3.5 cm heave distance. These parameters are similar to those established in experimental and computational studies of bluegill sunfish dorsal and anal fins (Akhtar et al., 2007; Drucker and Lauder, 2001). The left panels show the foils and water illuminated by a laser light sheet from top to bottom in these images; the foils cast shadows toward the bottom. Video sample rate was 500 Hz. In the right panel these images are analyzed to show water flow velocities and vorticity around the two foils (vectors were not calculated in the fin shadows), as in the previous analysis of the sunfish dorsal and anal fins (Fig. 4). A distinct thrust wake is visible at 0 ms. Notice how vorticity from Foil 1 impacts Foil 2 as it moves inline with the first foil at 110 ms (B). An attached leading edge vortex is visible on Foil 2 at 160 ms, enhanced by incoming vorticity from Foil 1. Note also that water flow in the gap between the two foils is nearly orthogonal to free stream flow at 0 and 160 ms, similar to flow patterns observed between the dorsal fin and tail in sunfish (Fig. 4). Every other vector is shown for clarity in the right column; images on the left have been contrast-enhanced.

Prospectus

The construction of robotic models that capture key features of the functional design of fishes promises to provide a significant new avenue for the exploration of longstanding questions in aquatic locomotion. Fish biorobotics, coupled with the ability to study the hydrodynamics of locomotion *in vivo*, provides a powerful intellectual combination for pursuing key questions in aquatic propulsion.

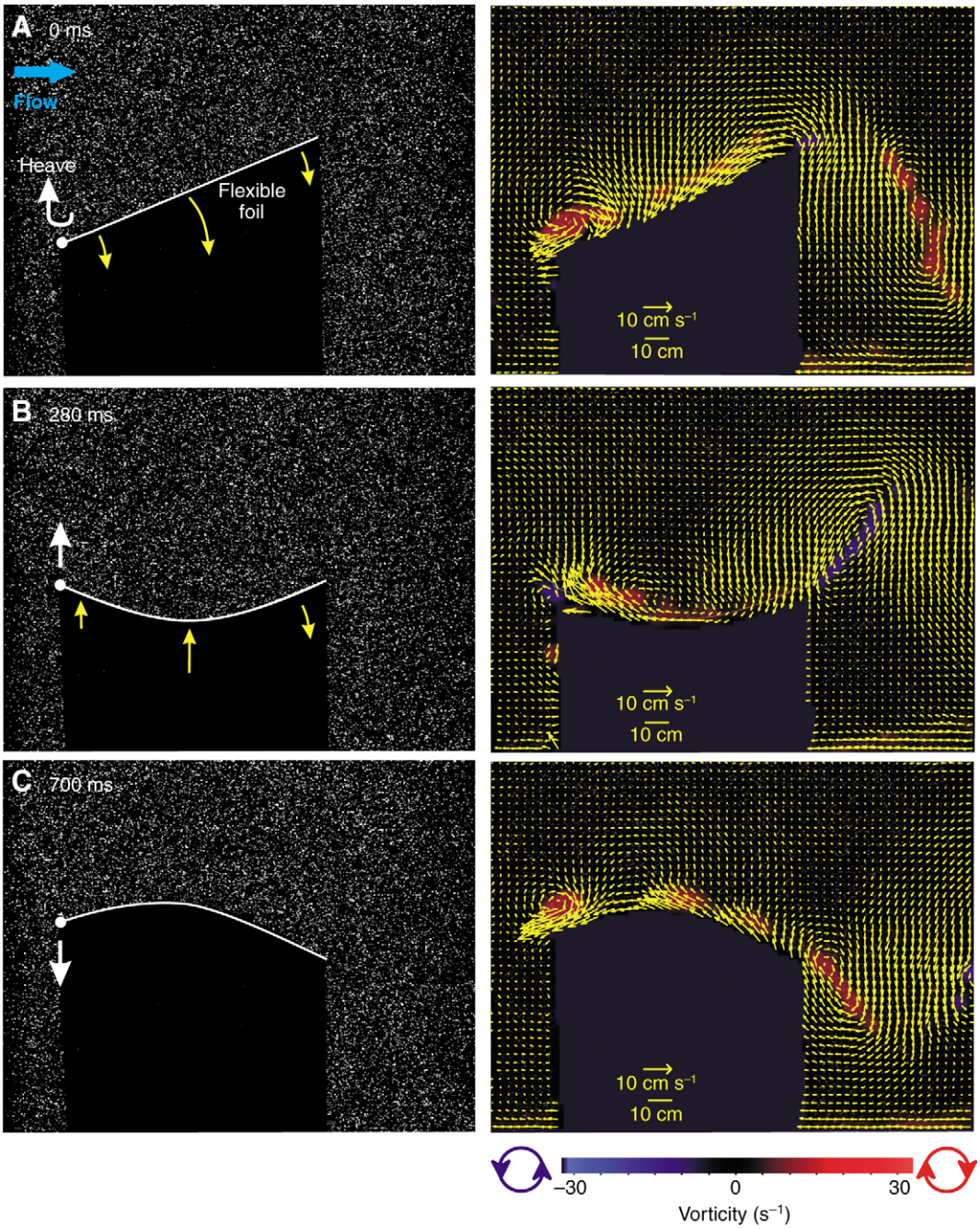

Fig. 10. Hydrodynamics of a single, flexible, flapping foil self-propelling at a speed of 24 cm s^{-1}. The white arrow shows the heave motion (3.5 cm heave amplitude) of the rod that actuates the flexible foil, composed of a plastic sheet of the same dimensions as the foils in Fig. 9. Foil thickness is 0.32 mm, foil length=19 cm, foil height=6.8 cm, and the video sample rate is 250 Hz. The left panels show the flexible foil and water illuminated by a laser light sheet from top to bottom; the flexible foil casts a shadow toward the bottom of each image; these images have been contrast-enhanced. Large yellow arrows in the left-hand panels show the direction of foil surface motion from one panel to the next. The actuating rod to which the foil is attached and the thin black foil itself have been enhanced by a white dot and line, respectively, for clarity. In the right panels these images are analyzed to quantify water flow velocities and vorticity around the flexible foil (vectors could not be calculated in the fin shadows), as in the previous analysis of two foil self-propulsion (Fig. 9). Note that an attached leading edge vortex (LEV) is visible at 0 ms as the foil leading edge nears the end of its downward motion and begins to move up. This attached LEV persists throughout the duration of the downstroke, until almost 930 ms (not shown). A distinct thrust wake is evident behind the flexible foil, with a strong side component.

The generality of the approach discussed here also indicates that many broader issues relating not just to fish propulsion but also to the design of aquatic organisms in general and underwater vehicle design using biologically inspired features, can be examined using biorobotic models (Bandyopadhyay, 2004; Fish, 2004; Long et al., 2006b; Miklosovic et al., 2004; Tangorra et al., 2007a; Tangorra et al., 2007b). The question of how flapping foils in series interact is a general one, with implications for flapping propulsion in both water and air, and the propulsive significance of flexibility, a hallmark of biological systems, is still not well understood. What do organisms gain in performance, if anything, by having flexible propulsors? New directions and questions require new approaches, and integrating the study of biorobotic models with experimental analyses of animals moving *in vivo* promises to be one such new avenue.

This work was supported by an ONR-MURI Grant N00014-03-1-0897 on fish pectoral fin function, monitored by Dr Thomas McKenna and initiated by Dr Promode Bandyopadhyay, and by NSF grant IBN0316675 to G.V.L. We thank Drs Rajat Mittal and Promode Bandyopadhyay for many helpful discussions on bio-inspired propulsion, Eric Tytell for his help in designing the dual flapping foil robot, Naomi Davidson for her many contributions to the pectoral fin robot, and Eliot Drucker for collaborative work on sunfish fin function. Two referees provided helpful suggestions on the manuscript. Karsten Hartel kindly provided the photograph in Fig. 1C. Tony Julius, Mary Hong and Julie Idlet provided invaluable assistance in the lab.

References

Akhtar, I., Mittal, R., Lauder, G. V. and Drucker, E. (2007). Hydrodynamics of a biologically inspired tandem flapping foil configuration. *Theor. Comput. Fluid Dyn.* **21**, 155-170.

Alben, S., Madden, P. G. A. and Lauder, G. V. (2007). The mechanics of active fin-shape control in ray-finned fishes. *J. R. Soc. Interface* **4**, 243-256.

Alexander, R. M. (1983). The history of fish mechanics. In *Fish Biomechanics* (ed. P. W. Webb and D. Weihs), pp. 1-35. New York: Praeger.

Alvarado, P. V. and Youcef-Toumi, K. (2005). Performance of machines with flexible bodies designed for biomimetic locomotion in liquid environments. In *Proceedings of the 2005 IEEE International Conference on Robotics and Automation, 18-22 April 2005*, pp. 3324-3329. Barcelona: IEEE. http://ieeexplore.ieee.org/servlet/opac?punumber=10495.

Anderson, J. M. and Chhabra, N. (2002). Maneuvering and stability performance of a robotic tuna. *Integr. Comp. Biol.* **42**, 118-126.

Arreola, V. and Westneat, M. W. (1997). Mechanics of propulsion by multiple fins: kinematics of aquatic locomotion in the burrfish (*Chilomycterus schoepfi*). *Philos. Trans. R. Soc. Lond. B Biol. Sci.* **263**, 1689-1696.

Bandyopadhyay, P. R. (2004). Biology-inspired science and technology for autonomous underwater vehicles. *IEEE J. Oceanic Eng.* **29**, 542-546.

Bandyopadhyay, P. R. (2005). Trends in biorobotic autonomous undersea vehicles. *IEEE J. Oceanic Eng.* **30**, 109-139.

Barrett, D. S., Triantafyllou, M. S., Yue, D. K. P., Grosenbaugh, M. A. and Wolfgang, M. J. (1999). Drag reduction in fish-like locomotion. *J. Fluid Mech.* **392**, 183-212.

Beal, D. N., Hover, F. S., Triantafyllou, M. S., Liao, J. and Lauder, G. V. (2006). Passive propulsion in vortex wakes. *J. Fluid Mech.* **549**, 385-402.

Biewener, A. (2003). *Animal Locomotion*. Oxford: Oxford University Press.

Breder, C. M. (1926). The locomotion of fishes. *Zoologica* **4**, 159-256.

Drucker, E. G. and Lauder, G. V. (1999). Locomotor forces on a swimming fish: three-dimensional vortex wake dynamics quantified using digital particle image velocimetry. *J. Exp. Biol.* **202**, 2393-2412.

Drucker, E. G. and Lauder, G. V. (2001). Locomotor function of the dorsal fin in teleost fishes: experimental analysis of wake forces in sunfish. *J. Exp. Biol.* **204**, 2943-2958.

Drucker, E. G. and Lauder, G. V. (2002). Wake dynamics and locomotor function in fishes: interpreting evolutionary patterns in pectoral fin design. *Integr. Comp. Biol.* **42**, 997-1008.

Drucker, E. G. and Lauder, G. V. (2005). Locomotor function of the dorsal fin in rainbow trout: kinematic patterns and hydrodynamic forces. *J. Exp. Biol.* **208**, 4479-4494.

Fish, F. (2004). Structure and mechanics of nonpiscine control surfaces. *IEEE J. Oceanic Eng.* **29**, 605-621.

Fish, F. and Lauder, G. V. (2006). Passive and active flow control by swimming fishes and mammals. *Annu. Rev. Fluid Mech.* **38**, 193-224.

Geerlink, P. J. and Videler, J. J. (1974). Joints and muscles of the dorsal fin of *Tilapia nilotica* L. (Fam. Cichlidae). *Neth. J. Zool.* **24**, 279-290.

Gray, J. (1953). *How Animals Move*. Cambridge: Cambridge University Press.

Houssay, F. (1912). *Forme, Puissance et stabilité des Poissons*. Paris: Herman.

Hove, J. R., O'Bryan, L. M., Gordon, M. S., Webb, P. W. and Weihs, D. (2001). Boxfishes (Teleostei: Ostraciidae) as a model system for fishes swimming with many fins: kinematics. *J. Exp. Biol.* **204**, 1459-1471.

Hover, F. S., Haugsdal, O. and Triantafyllou, M. S. (2004). Effect of angle of attack profiles in flapping foil propulsion. *J. Fluid Struct.* **19**, 37-47.

Jayne, B. C., Lozada, A. and Lauder, G. V. (1996). Function of the dorsal fin in bluegill sunfish: motor patterns during four locomotor behaviors. *J. Morphol.* **228**, 307-326.

Kato, N. (2000). Control performance in the horizontal plane of a fish robot with mechanical pectoral fins. *IEEE J. Oceanic Eng.* **25**, 121-129.

Lauder, G. V. (1982). Structure and function of the caudal skeleton in the pumpkinseed sunfish, *Lepomis gibbosus*. *J. Zool. Lond.* **197**, 483-495.

Lauder, G. V. (1989). Caudal fin locomotion in ray-finned fishes: historical and functional analyses. *Am. Zool.* **29**, 85-102.

Lauder, G. V. (2006). Locomotion. In *The Physiology of Fishes*. 3rd edn (ed. D. H. Evans and J. B. Claiborne), pp. 3-46. Boca Raton: CRC Press.

Lauder, G. V. and Drucker, E. G. (2002). Forces, fishes, and fluids: hydrodynamic mechanisms of aquatic locomotion. *News Physiol. Sci.* **17**, 235-240.

Lauder, G. V. and Drucker, E. G. (2004). Morphology and experimental hydrodynamics of fish fin control surfaces. *IEEE J. Oceanic Eng.* **29**, 556-571.

Lauder, G. V. and Madden, P. G. A. (2006). Learning from fish: kinematics and experimental hydrodynamics for roboticists. *Int. J. Autom. Comput.* **4**, 325-335.

Lauder, G. V. and Tytell, E. D. (2006). Hydrodynamics of undulatory propulsion. In *Fish Biomechanics: Fish Physiology*. Vol. 23 (ed. R. E. Shadwick and G. V. Lauder), pp. 425-468. San Diego: Academic Press.

Lauder, G. V., Nauen, J. C. and Drucker, E. G. (2002). Experimental hydrodynamics and evolution: function of median fins in ray-finned fishes. *Integr. Comp. Biol.* **42**, 1009-1017.

Lauder, G. V., Madden, P. G. A., Mittal, R., Dong, H. and Bozkurttas, M. (2006). Locomotion with flexible propulsors I: experimental analysis of pectoral fin swimming in sunfish. *Bioinspir. Biomim.* **1**, S25-S34.

Liu, J.-D. and Hu, H. (2006). Biologically inspired behaviour design for autonomous robotic fish. *Int. J. Autom. Comput.* **3**, 336-347.

Liu, J., Dukes, I. and Hu, H. (2005). Novel mechatronics design for a robotic fish. In *2005 IEEE/RSJ International Conference on Intelligent Robots and Systems, 2-6 August 2005*, pp. 807-812. doi: 10.1109/IROS.2005.1545283. http://ieeexplore.ieee.org/Xplore/guesthome.jsp.

Long, J. H., Jr, Koob, T. J., Irving, K., Combie, K., Engel, V., Livingston, N., Lammert, A. and Schumacher, J. (2006a). Biomimetic evolutionary analysis: testing the adaptive value of vertebrate tail stiffness in autonomous swimming robots. *J. Exp. Biol.* **209**, 4732-4746.

Long, J. H., Schumacher, J., Livingston, N. and Kemp, M. (2006b). Four flippers or two? Tetrapodal swimming with an aquatic robot. *Bioinspir. Biomim.* **1**, 20-29.

Low, K. H. (2006). Locomotion and depth control of robotic fish with modular undulating fins. *Int. J. Autom. Comput.* **3**, 348-357.

Miklosovic, D. S., Murray, M. M., Howle, L. E. and Fish, F. E. (2004). Leading-edge tubercles delay stall on humpback whale (*Megaptera novaeangliae*) flippers. *Phys. Fluids* **16**, L39-L42.

Mittal, R., Dong, H., Bozkurttas, M., Lauder, G. V. and Madden, P. G. A. (2006). Locomotion with flexible propulsors II: computational modeling and analysis of pectoral fin swimming in sunfish. *Bioinspir. Biomim.* **1**, S35-S41.

Nauen, J. C. and Lauder, G. V. (2002a). Hydrodynamics of caudal fin locomotion by chub mackerel, *Scomber japonicus* (Scombridae). *J. Exp. Biol.* **205**, 1709-1724.

Nauen, J. C. and Lauder, G. V. (2002b). Quantification of the wake of rainbow trout (*Oncorhynchus mykiss*) using three-dimensional stereoscopic digital particle image velocimetry. *J. Exp. Biol.* **205**, 3271-3279.

Shadwick, R. E. and Lauder, G. V. (ed.) (2006). *Fish Biomechanics: Fish Physiology*, *Vol. 23*. San Diego: Academic Press.

Standen, E. M. and Lauder, G. V. (2005). Dorsal and anal fin function in bluegill sunfish (*Lepomis macrochirus*): three-dimensional kinematics during propulsion and maneuvering. *J. Exp. Biol.* **205**, 2753-2763.

Standen, E. M. and Lauder, G. V. (2007). Hydrodynamic function of dorsal and anal fins in brook trout (*Salvelinus fontinalis*). *J. Exp. Biol.* **210**, 325-339.

Tangorra, J., Anquetil, P., Fofonoff, T., Chen, A., Del Zio, M. and Hunter, I. (2007a). The application of conducting polymers to a biorobotic fin propulsor. *Bioinsp. Biomimet.* **2**, S6-S17.

Tangorra, J. L., Davidson, S. N., Hunter, I. W., Madden, P. G. A., Lauder, G. V., Dong, H., Bozkurttas, M. and Mittal, R. (2007b). The development of a biologically inspired propulsor for unmanned underwater vehicles. *IEEE J. Oceanic Eng.* In press.

Techet, A. H., Hover, F. S. and Triantafyllou, M. S. (1998). Vortical patterns behind a tapered cylinder oscillating transversely to a uniform flow. *J. Fluid Mech.* **363**, 79-96.

Triantafyllou, M. S. and Triantafyllou, G. S. (1995). An efficient swimming machine. *Sci. Am.* **272**, 64-70.

Tytell, E. D. (2006). Median fin function in bluegill sunfish, *Lepomis macrochirus*: streamwise vortex structure during steady swimming. *J. Exp. Biol.* **209**, 1516-1534.

Tytell, E. D. and Lauder, G. V. (2004). The hydrodynamics of eel swimming. I. Wake structure. *J. Exp. Biol.* **207**, 1825-1841.

Webb, P. (2006). Stability and maneuverability. In *Fish Biomechanics: Fish Physiology.* Vol. 23 (ed. R. E. Shadwick and G. V. Lauder), pp. 281-332. San Diego: Academic Press.